The Astrophysical Journal, 705:670–682, 2009 November 1 doi:10.1088/0004-637X/705/1/670

THE LOCAL DUST FOREGROUNDS IN THE MICROWAVE SKY. I. THERMAL EMISSION SPECTRA

Valeri Dikarev[1,3,5], Oliver Preuss[1], Sami Solanki[1,4], Harald Krüger[1,5], and Alexander Krivov[2]
[1] Max-Planck-Institut für Sonnensystemforschung, 37191 Katlenburg-Lindau, Germany
[2] Friedrich-Schiller Universität Jena, Germany
[3] The University of Bielefeld, Universitätsstraße 25, 33615 Bielefeld, Germany
[4] School of Space Research, Kyung Hee University, Yongin, Gyeonggi 446-771, Korea
Received 2009 April 6; accepted 2009 September 15; published 2009 October 14

ABSTRACT

Analyses of the cosmic microwave background (CMB) radiation maps made by the *Wilkinson Microwave Anisotropy Probe* (*WMAP*) have revealed anomalies not predicted by the standard inflationary cosmology. In particular, the power of the quadrupole moment of the CMB fluctuations is remarkably low, and the quadrupole and octopole moments are aligned mutually and with the geometry of the solar system. It has been suggested in the literature that microwave sky pollution by an unidentified dust cloud in the vicinity of the solar system may be the cause for these anomalies. In this paper, we simulate the thermal emission by clouds of spherical homogeneous particles of several materials. Spectral constraints from the *WMAP* multi-wavelength data and earlier infrared observations on the hypothetical dust cloud are used to determine the dust cloud's physical characteristics. In order for its emissivity to demonstrate a flat, CMB-like wavelength dependence over the *WMAP* wavelengths (3 through 14 mm), and to be invisible in the infrared light, its particles must be macroscopic. Silicate spheres of several millimeters in size and carbonaceous particles an order of magnitude smaller will suffice. According to our estimates of the abundance of such particles in the zodiacal cloud and trans-Neptunian belt, yielding the optical depths of the order of 10^{-7} for each cloud, the solar system dust can well contribute 10 μK (within an order of magnitude) in the microwaves. This is not only intriguingly close to the magnitude of the anomalies (about 30 μK), but also alarmingly above the presently believed magnitude of systematic biases of the *WMAP* results (below 5 μK) and, to an even greater degree, of the future missions with higher sensitivities, e.g., *Planck*.

Key words: cosmic microwave background – diffuse radiation – interplanetary medium – meteors, meteoroids – radiation mechanisms: thermal

1. INTRODUCTION

The five-year release (Hinshaw et al. 2009) of the *Wilkinson Microwave Anisotropy Probe* (*WMAP*; Bennett et al. 2003a) data represents the current highlight of a project which provided a so far unprecedented amount of high-precision cosmological data. On small angular scales the measurement of the cosmic microwave background (CMB) anisotropies led to the precise confirmation of the Λ-cold dark matter (ΛCDM) model of a nearly spatially flat universe, dominated by dark energy and non-baryonic dark matter (Spergel et al. 2006). Nevertheless at large scales a number of unexpected, potentially damaging anomalous features in the CMB have been reported, indicating that either our current understanding of standard inflationary cosmology or the data processing, including foreground removal techniques is as yet inadequate.

Among these anomalies, the expansion of the CMB sky in spherical harmonic functions resulted in an octopole which is unusually planar and oriented parallel to the quadrupole (Tegmark et al. 2003; de Oliveira-Costa et al. 2004). Three of the four planes determined by the quadrupole and octopole are orthogonal to the ecliptic at 99.1% confidence level (CL), and the normals to these planes are aligned with the direction of the cosmological dipole and with the equinoxes, inconsistent with Gaussian random, statistically isotropic skies at 99.8% CL (Schwarz et al. 2004).

The presence of non-Gaussian features in the CMB temperature fluctuations was reported by Copi et al. (2004). Land & Magueijo (2005) suggested that the presence of preferred directions in the low-order multipoles also extends to higher multipoles beyond the octopole.

Of course, any of these anomalies challenges the validity of the standard scenario of inflationary cosmology which predicts scale-free, statistically isotropic, and Gaussian random CMB temperature fluctuations and uncorrelated multipoles. However, although it is very unlikely that these features are just a statistical fluke, their cosmological origin is still an open debate. Therefore, besides various kinds of potential new physics (Hannestad & Mersini-Houghton 2005; Moffat 2005; Jaffe et al. 2005; Gordon et al. 2005), a compact cosmic topology (de Oliveira-Costa et al. 2004; Mota et al. 2004; Cornish et al. 2004) or modified inflation (Piao 2005; Linde 2004; Hunt & Sarkar 2004) and also conventional effects of Galactic foreground emission (Eriksen et al. 2004; Slosar & Seljak 2004; Naselsky et al. 2005) have been suggested as possible physical explanations.

The significance of the correlations of the quadrupole and octopole with the ecliptic plane, however, hints at the solar system as the origin of an unaccounted bias (Schwarz et al. 2004; Copi et al. 2006). Starkman and Schwarz (2005) speculated that an unknown dark cloud of dust in the solar neighborhood may have contributed to the microwave sky surveyed by the *WMAP*. Frisch (2005) proposed that the interstellar dust trapped magnetically in the heliosphere can possibly explain the CMB anomalies. Babich et al. (2007) discussed the possibility of discovering the dust of the trans-Neptunian belt in the *WMAP* data. None of the investigations, however, gave fully convincing explanations to solve the problem of the CMB anomalies.

This paper opens a series of publications in which we simulate the microwave thermal emission of dust clouds inside or in

[5] Guest scientist at Max-Planck-Institut für Kernphysik, Heidelberg, Germany.

the vicinity of the solar system, and test whether these clouds can be responsible for the unexplained correlations or can be discovered in the CMB experiment data. Here we focus on the spectral constraints on material and size distribution of the particles forming a cloud invisible in the infrared wavelengths and imitating closely the CMB emission in the microwaves. Such cloud would indeed contribute to the CMB maps without us knowing about it. The absolute photometry and spatial geometry of candidate clouds' contributions to the CMB maps are left for further scrutiny in follow-up studies.

The paper is organized as follows. Section 2 deals with the general constraints on an unknown cloud's spectrum from the infrared wavelengths to microwaves. It shows how a cloud of macroscopic particles can be noticeable in the microwaves and still avoid detection in the infrared light. Candidate clouds are proposed in the solar system that can add non-negligible emission in the microwaves without being easily recognized in the infrared light. Estimates of the microwave temperatures of some known dust clouds are made, supporting the case for a detailed study. Constraints on the microwave spectra of foreground sources from the Internal Linear Combination (ILC) maps derived from the *WMAP* multi-wavelength data (Bennett et al. 2003b) are also formulated to facilitate the determination of plausible composition and size distribution of the cloud. Section 3 introduces the elements of the Mie theory of light scattering necessary for our calculations of the thermal emission from dust particles, and borrows bibliographic sources on the optical properties of several chemical compositions from the database (Henning et al. 1999). Thermal emission spectra of various sample and one natural dust clouds are generated in Section 4 and tested against the constraints placed by the ILC maps. Conclusions are drawn in Section 5.

2. THE THERMAL EMISSION DUE TO A FOREGROUND CLOUD

2.1. In the Infrared Wavelengths

The first strong spectral constraint on the hypothetical dust cloud comes from the fact that so far it has not been recognized at other wavelengths, particularly in the infrared light, where dust is normally very bright. This is true e.g., for the zodiacal thermal emission produced predominantly by dust with temperatures around 300 K and peaking at $\sim$10 μm, and even for the Galactic dust with temperatures around 10 K with a maximum radiance in the far-infrared. However, these clouds are composed of particles much smaller than a millimeter in size, and in this section we demonstrate how a cloud of bigger particles can avoid detection in the infrared light and still shine considerably bright in the microwaves.

Figure 1 compares intensities of the CMB radiation, its average anisotropy, and several dust clouds between wavelengths of 10 to 3×10^4 μm. The emissivity of interplanetary dust ("IPD") is simplified to unity below 100 μm and λ^{-2} above this wavelength (cf. Leinert et al. 1983). This is an approximation to e.g., astronomical silicate by Draine & Lee (1984) and the Grün et al. (1985) model of interplanetary dust in which the bulk of cross-sectional area is comprised by the meteoroids from 10 to 100 μm in size. Maris & Burigana (2007) used a similar law in their analysis of the microwave emission by interplanetary dust. The other clouds on the plot are hypothetical, with the constituent particles being macroscopic with respect to all wavelengths, i.e., having flat emissivities from the infrared to millimeter wavelength. Their geometrical optical depths τ were set so as to provide an extra temperature of 30 μK in the microwaves, i.e., close to the magnitudes of the CMB quadrupole and octopole.

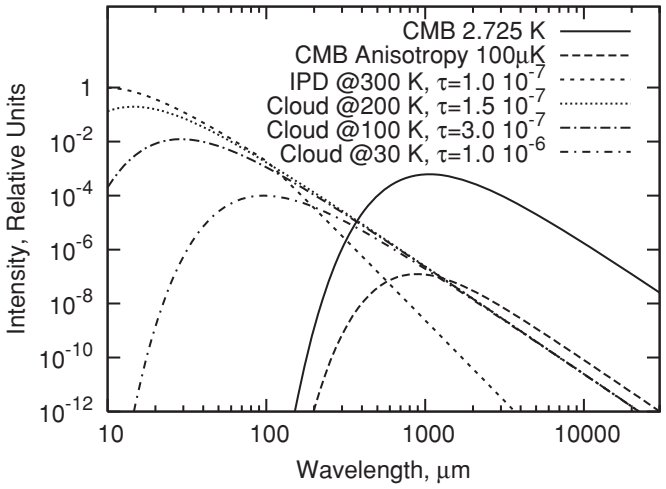

Figure 1. Relative intensities of the CMB radiation, its anisotropy, and sample dust clouds. "IPD" stands for interplanetary dust which is assumed to have a flat unit emissivity below 100 μm and an emissivity $\propto \lambda^{-2}$ above this wavelength, i.e., roughly that of astronomical silicate (Draine & Lee 1984) for 10–100 μm sized interplanetary particles which are dominant in the meteoroid flux at 1 AU from the Sun (Grün et al. 1985), when weighted by their cross-sectional area (cf. Leinert et al. 1998). "Clouds" have flat unit emissivities from the infrared wavelengths to the microwaves, i.e., are composed of the macro-meteoroids big with respect to all wavelengths displayed. Their temperatures are determined by their heliocentric distances ($\sim$300 K at 1 AU, 200 K at 2 AU, 100 K at 9 AU, and 30 K at 100 AU; see Equation (7) in the text). The geometrical optical depth τ of "clouds" is calculated so as to provide an excess temperature of 30 μK in the microwaves. The optical depth of "IPD" is 10^{-7}.

The interplanetary dust at 300 K is the brightest source in the infrared light. The CMB radiation exceeds the emission from interplanetary dust above 300 μm wavelength, while the corresponding threshold wavelength for the CMB anisotropy is 600 μm. In the *WMAP* wavelength range (above 3 mm), the interplanetary dust is three or more orders of magnitude dimmer than the CMB anisotropy, explaining why it had not been taken into account as a serious bias. However, the steep decline of interplanetary dust in Figure 1 with wavelength increase is due to its presumed emissivity $\propto \lambda^{-2}$ above $\lambda = 100$ μm. Clouds of macroscopic particles naturally do not follow this trend.

Figure 1 allows one to put constraints on the temperature and optical depth of the unknown cloud that is seen in the microwaves but as yet has not been recognized in the infrared light. Obviously, it must not be brighter than the interplanetary dust in the infrared wavelengths between 10 and 100 μm, where the zodiacal thermal emission is dominant. This criterion is met by all "clouds" in the plot, and even a cloud of macro-meteoroids at 300 K, i.e., an equilibrium dust temperature near Earth (see Equation (7) in text below, or refer to Reach 1988), would not be immediately rejected.

This criterion may look too bold: even if the cloud mimics really well the emission maps of smaller interplanetary dust particles, its addition would double the total brightness. However, Reach (1988) found that the infrared emission predictions based on the Grün et al. (1985) model are half the *IRAS* observations. Thus, a considerable degree of freedom persists in interpreting the infrared observations using the size distribution of Grün et al. (1985), even before any exotic hypothesis is suggested, e.g., a local enhancement of dust around *WMAP* near the L_2 point of Sun–Earth which has been hidden from the earlier sufficiently

sensitive observatories like *IRAS* and *COBE* at solar elongations $> 135^{\circ}$.

Figure 1 can provide only an upper limit on the cloud's brightness. An estimate of the lower limit is more difficult to obtain since our knowledge about big meteoroids away from the Earth orbit is rather poor. Sykes & Walker (1992) estimate the optical depth of a cometary dust trail as 10^{-8} (10P/Tempel 2), and provide evidence that the constituent particles are cm-sized. At 250 K, the trail is 2.5 μK bright in the microwaves. Similar estimates can be obtained for asteroid dust belts, if they are composed of particles with a unit emissivity (Low et al. 1984). These structural elements are recognized as faint but distinct features in the smooth background zodiacal emission ($\tau \sim 10^{-7}$). If there were broader structures—in space or on celestial maps—resembling the smaller interplanetary grain distribution, they could be easily confused with the zodiacal thermal emission in the infrared wavelengths. In what follows, we present two plausible candidates, concentrated between Earth and Jupiter and in the trans-Neptunian belt.

The Grün et al. (1985) model is based largely on the data acquired near Earth, most notably the lunar rock samples covered by plentiful micro-craters. They provide a vast amount of information for the model's meteoroid mass distribution inferred over 20 orders of magnitude (10^{-18} to 10^{2} g), however, the Moon spins, erasing memory of the direction of impacts, and it samples a very limited volume in the solar system space. There is just a little clue, therefore, as to where these meteoroids came from and to what extent they are representative of the entire solar system. Populations of particles have been known to exist which are not sampled by the Moon, with the compositions and sizes not resembling those of the Earth-crossing meteoroids. Examples include the above-mentioned asteroid dust bands and cometary trails. Meteoroid streams should exist along the orbits of the comets with the perihelia outside 1 AU from the Sun, just as they exist along the comet orbits crossing the Earth's orbit, revealed by meteor showers. Low number densities and fluxes of these particles have so far prevented their direct and remote registration outside the Earth–Moon system. Theoretical modeling is necessary to attempt to fulfill this observational gap.

Hughes & McBride (1990) simulated the number density distribution of meteoroids from short-period comets by distributing test particles uniformly in mean anomaly along each comet's orbit. Most of these particles never cross the Earth's orbit. Their number density peaks at 2–2.5 AU and exceeds its modest near-Earth level up to 5.5 AU (Figure 2). The near-Earth level is about 5 times lower than the maximum. If their parent comets were the only source of big meteoroids (>100 μm in size) reaching Earth and Moon, they would constitute about 10% of the total cross-sectional area of meteoroids in the Grün et al. (1985) model of the flux at 1 AU (see also Figure 6 in Section 3.3). As the total optical depth of the zodiacal cloud is $\sim 10^{-7}$, and if its size distribution were spatially homogeneous, then these particles would contribute an optical depth of just $\sim 10^{-8}$.

However, the Poynting–Robertson drag (Wyatt & Whipple 1950; Leinert et al. 1983; Gor'kavyi et al. 1997) causes a drift of small meteoroids toward the Sun and a depletion of these particles with heliocentric distance $\propto R^{-1}$ or steeper. The simulation by Hughes & McBride (1990) shows that big meteoroids do not follow this trend. In their model, assuming Keplerian motion, the large particles reside near the parent comet orbits. Although this assumption is only accurate if the planetary perturbations are ignored, by including a large ensemble of comets (135 in Hughes & McBride 1990) one can initially account for

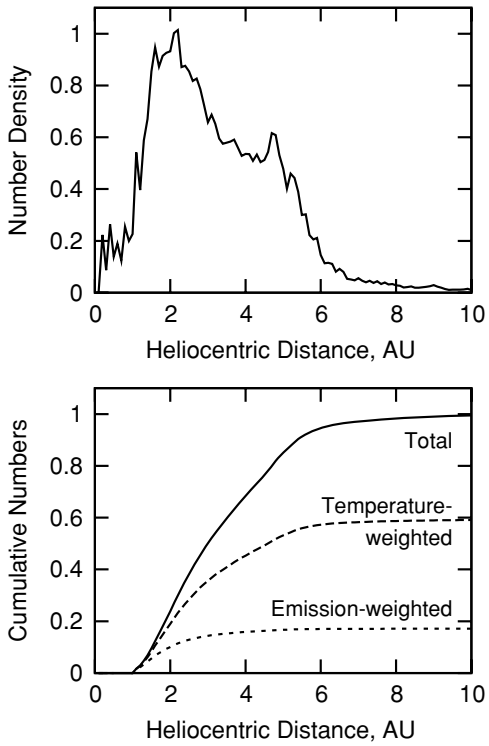

Figure 2. Radial number densities (top) and cumulative numbers (bottom) of meteoroids from short-period comets on the anti-solar line of sight from Earth (cf. Hughes & McBride 1990). All comet orbits were populated by an equal number of particles distributed uniformly in mean anomaly. The cumulative numbers use the number density as it is (upper curve), with a normalization to 1 at 10 AU, then the density weighted by the equilibrium meteoroid temperature (middle curve) proportional to the inverse square root of the distance (see Reach 1988, or the text below), and then the density weighted by the total emission (lower curve) proportional to the inverse square distance. An observation sensitive to the total emission (in visual or infrared light) is inefficient to discover meteoroids along the short-period comet orbits. A temperature-sensitive observation (in the microwaves, where the meteoroids emit in the Rayleigh–Jeans regime with an intensity proportional to temperature) reveals remote dust clouds much better.

the planetary perturbations already imprinted in the cometary orbit distribution (ignoring the observational selection effects on comets). More sophisticated modeling of the sources and evolution of meteoroids taking the Poynting–Robertson effect and mutual collisions into account by Ishimoto (2000) independently confirms that the number of big meteoroids is indeed considerably higher outside 1 AU.

Now let us try to estimate the microwave emission from the big particles based on Figure 2. The total optical depth of zodiacal cloud is based on measurements confined to the vicinity of the Earth's orbit: the total thermal emission as well as visual light reflected by an interplanetary meteoroid illuminated by the Sun decreases with the heliocentric distance R sharply: $\propto R^{-2}$ (i.e., proportional to the incident radiation flux). The number density of small meteoroids (less than $\sim$ 100 μm in size) dominating the cross-sectional area of the zodiacal cloud according to the model by Grün et al. (1985) also decreases $\propto R^{-1}$ or steeper. Thus, three quarters of the total thermal emission observed e.g., in the anti-solar direction should come from within 1 AU from the Earth. The emission-weighted cumulative numbers in Figure 2 show that for the cometary meteoroids of Hughes & McBride (1990) one-half of the radiation would come from within 1 AU outside the Earth's orbit (divide the emission-weighted cumulative number at 10 AU by

that at 2 AU): their number density initially grows with distance rather than decays.

In the microwaves, the thermal emission from dust particles is in the Rayleigh–Jeans regime and is proportional to temperature. The temperature decrease with the distance is rather slow, $\propto R^{-1/2}$ (see e.g., Reach 1988, or refer to the following section of this paper for a derivation). Thus, more distant particles are revealed, including virtually all of the Hughes & McBride (1990) meteoroids, whereas the small particles of the Grün et al. (1985) model are still depleted at longer distances due to the Poynting–Robertson drag.

If indeed the optical depth of the big meteoroids was $\sim 10^{-8}$ for the observations sensitive to the emission from dust within 1 AU from the Earth, the model by Hughes & McBride (1990) predicts that all meteoroids from short-period comets (including those beyond 2 AU from the Sun) would have a depth of about 5×10^{-8}. A scaling factor of 5 stems from the total cumulative number plot in Figure 2, which shows that only 1/5 of the Hughes & McBride (1990) particles are located within 1 AU from the Earth. However, even some of these particles will be hidden to an Earth-bound microwave observer due to a slow temperature decrease. The temperature-weighted cumulative number restricts the scaling factor to 3 for the microwave range of wavelengths.

Note that the base value of $\sim 10^{-8}$ for the total optical depth of big meteoroids within 1 AU from Earth in the anti-solar direction is itself derived from the Grün et al. (1985) model adjusted to the meteoroid flux at 1 AU from the Sun strictly. In the Hughes & McBride (1990) model, the number density of the big meteoroids is 2–3 times higher, on average, between 1 and 2 AU from the Sun, than at the Earth orbit (Figure 2). This allows one to raise the base value accordingly and to come to the total temperature-weighted depths between 6×10^{-8} and 9×10^{-8}. This is in fact comparable with the visual optical depth of 10^{-7} of the zodiacal cloud. At 150–300 K, these meteoroids could add 9–27 μK emission in the microwaves, provided that they have a flat unit emissivity from the infrared wavelengths to microwaves, and without being immediately resolvable in infrared radiation (and very likely in visual light too, depending though on the particle albedo).

The assumption of Hughes & McBride (1990) of an equal meteoroid number per comet orbit can be challenged. The production rates tend to be higher for low-perihelion comets and the lifetimes tend to be longer for high-aphelion comets. One can thus argue that if a few active comets, such as 1P/Halley or 2P/Encke, produce more dust than all others, or some particular comet orbits allow for longer survival times, this in fact will only raise our estimate. We used an implicit assumption that the emission map of the big meteoroids is broadly as smooth as that of the zodiacal cloud. If a single bright comet is responsible, then the distribution is strongly biased toward its aphelion where the particles in Keplerian orbits stay much longer. They would produce a smaller and brighter spot on the sky. This is especially relevant to the Halley-type, long-period, and Kreutzer-group comets ("sun-grazers").

There is another candidate cloud never observed in the microwaves: millimeter-sized meteoroids in the trans-Neptunian belt. Based on thermal emission models of debris disks of Krivov et al. (2008), we have estimated the microwave temperatures, although an uncertainty of one order of magnitude should be borne in mind. Table 1 lists the optical depths of the trans-Neptunian belt particles of four size ranges. The particles, which are macroscopic with respect to the microwaves (from 1 cm and above in size), have a total depth of 2×10^{-7}. At a temperature of $\sim$50 K, they would add $\sim$10 μK if their absorption efficiency were $Q_{\rm abs} \sim 1$. When the particles of all sizes above 1 mm are included, the total extra temperature is as high as $\sim$35 μK. In the infrared light, however, the trans-Neptunian belt is far too dim: taking all dust grains bigger than 10 μm into consideration, we obtain a total optical depth of $\sim 10^{-5}$, i.e., two orders of magnitude higher than that of the zodiacal cloud. However, the total blackbody emission at $\sim$30 AU from the Sun is 3 orders of magnitude smaller than near 1 AU (see Equation (7) below), hence the total thermal emission from the trans-Neptunian belt seen from Earth in the anti-solar direction is no more than 10% of that of the zodiacal cloud.

Table 1
Geometrical Optical Depths of the Trans-Neptunian Belt for an Observer Located in the Inner Solar System

Particle Size From	To	τ
10 μm	100 μm	5×10^{-6}
100 μm	1 mm	2×10^{-6}
1 mm	1 cm	5×10^{-7}
1 cm	∞	2×10^{-7}

Note. Estimates are based on debris disk models by Krivov et al. (2008) and the total belt mass of 0.02 $M_\oplus$ (Fuentes & Holman 2008).

Even if all or some of these particles are not the reason for the *WMAP* anomaly, e.g., due to their emissivities below unity, they cannot be totally disregarded, especially in the next generation CMB experiments.

2.2. In the Microwaves

Another spectral constraint comes from the microwave observations with *WMAP* which do not reveal any significant unknown foreground. As the CMB fluctuations are studied in terms of the effective temperature rather than radiance, let us first describe the conversion details, and introduce the notation of the temperature spectrum of a dust cloud.

A dust cloud of the temperature $T_{\rm D}$ and the column absorption area $\sigma(\lambda)$ at a given wavelength λ adds a specific energy flux $B_\lambda(T_{\rm D})\sigma(\lambda)$ to the cosmic microwave background radiation, which is at the average temperature of $T = 2.725$ K, given by $B_\lambda(T)$. In the CMB studies, their sum is usually described by the excess temperature ΔT_λ of an imaginary blackbody emission source that would emit the same flux, i.e., $B_\lambda(T + \Delta T_\lambda) = B_\lambda(T) + B_\lambda(T_{\rm D})\sigma(\lambda)$. When solved for ΔT_λ, this equation provides one with a handy formula

$$\Delta T_\lambda = \frac{hc}{k\lambda} \Big/ \ln\left[1 + \frac{E_\lambda(T)E_\lambda(T_{\rm D})}{E_\lambda(T_{\rm D}) + \sigma E_\lambda(T)}\right] - T, \qquad (1)$$

where $E_\lambda(T) = \exp(hc/kT\lambda) - 1$ comes from the Planck law, h and k are the Planck and Boltzmann constants (cf. Finkbeiner et al. 1999, who used an approximation working well only in the far-infrared and microwaves).

In the Rayleigh–Jeans regime, i.e., when $\lambda \gg hc/kT$ at long wavelength, the spectral radiance $B_\lambda(T)$ is approximated by $R_\lambda(T) = 2kT/c\lambda^4$ and a simple linear scaling is permitted: $\Delta T_\lambda = \sigma(\lambda)T_{\rm D}$. It will be used for rough estimates of the excess temperatures due to dust clouds in Section 2.1 only.

In general, instead of $B_\lambda(T + \Delta T_\lambda)$ simply ΔT_λ is given, so that the excess temperature can be plotted in the form of a spectrum. Temperature spectra of the CMB anisotropy

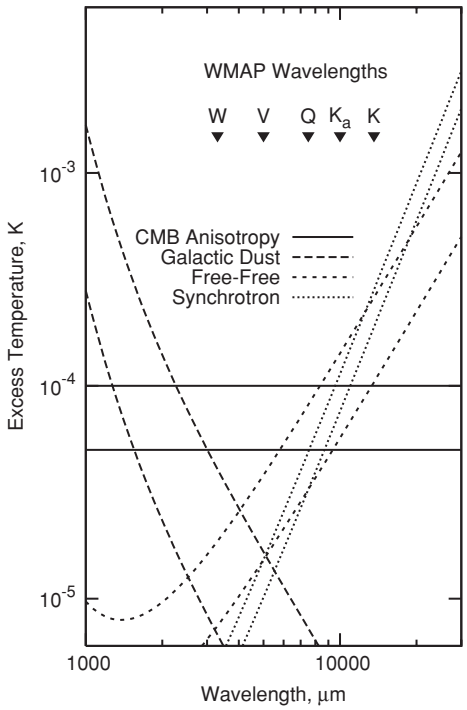

Figure 3. Excess temperatures of the CMB anisotropy and known foregrounds, relative to the CMB average temperature ($T = 2.725$ K), including the thermal emission by galactic dust, free–free emission arising from electron–ion scattering, and synchrotron emission due to the acceleration of cosmic ray electrons in magnetic fields (Bennett et al. 2003b). Shown are the upper and lower limits taken from these authors as the three foregrounds vary across the sky.

and several known foregrounds are shown in Figure 3. The foregrounds are the thermal emission from galactic dust, and free–free and synchrotron emissions arising, respectively, from the electron–ion scattering and acceleration of cosmic ray electrons in magnetic fields. It is clearly seen that the CMB anisotropy is dominant between 3 and 6 mm, whereas at other wavelengths either galactic dust or free–free and synchrotron emissions are more intensive.

Even inside the range of its dominance from 3 to 6 mm, the CMB anisotropy must be cleaned of the foregrounds. Several methods have been developed to perform this task. One method is to obtain precise maps of foregrounds at the wavelengths where they dominate, refine them based on relevant physical theories, extrapolate to the *WMAP* wavelengths and subtract them from the *WMAP* data (Hinshaw et al. 2007). For example, the galactic dust emission was mapped using the *IRAS* and *COBE* observations in infrared light, cleaned from the zodiacal dust emission by removing everything that is not correlated with the galactic hydrogen emission map, and then extrapolated to the microwaves assuming traditionally the emissivity law λ^{-2} (Schlegel et al. 1998). This method has the caveat of not knowing every foreground or everything about the physics of known foregrounds.

In contrast, the idea of the ILC method (Bennett et al. 2003b) is to reduce foreground and noise as far as possible by weighted linear combinations of multi-frequency data without using any special assumptions about particular spatial structures of the foregrounds. Suppose the thermodynamic temperature of map i and wavelength λ_i can be written as a sum of the CMB and the foreground temperature

$$T_{\rm sky}(\lambda_i) = T + \Delta T_f(\lambda_i), \tag{2}$$

the CMB maps are reconstructed by co-adding the data from the five *WMAP* wavelengths (3.3, 5.0, 7.5, 10.0, and 13.6 mm)

$$T_{\rm sky} = \sum_{i=1}^{k} w_i (T + \Delta T_f(\lambda_i)) = T + \sum_{i=1}^{k} w_i \Delta T_f(\lambda_i), \tag{3}$$

with the constraint that the weights w_i add to one in order to preserve only signals with a thermal CMB spectrum, i.e.,

$$\sum_{i=1}^{k} w_i = 1. \tag{4}$$

Since the emission of various foregrounds like free–free, synchrotron, and dust emission shows significant spatial variation, mainly along the Galactic plane, it is clear that also the weights w_i cannot be held constant across the whole sky. Hence, to accommodate the spectral variability of the foregrounds, the entire sky has been divided into 12 separate regions, within which the weights are constant and determined independently by the criterion that the weights have to minimize the variance

$$\mathrm{Var}(T_{\rm sky}) = \mathrm{Var}(T) + \mathrm{Var}\left(\sum_{i=1}^{k} w_i \Delta T_f(\lambda_i)\right), \tag{5}$$

so that the influence of the foreground emission is suppressed down to a minimum. The regions have been chosen such that 10 of them cover the inner Galactic plane, while the outer Galactic plane as well as higher Galactic latitudes are covered each by only one region. Since the weights are constant within each region, it follows that also any foreground emission, especially outside the Galactic plane, should have a constant spectrum throughout the region. Therefore, if this ILC assumption of a constant spectrum turns out to be inappropriate, e.g., because of an unknown dust cloud, the segmentation of the sky, especially outside the Galactic plane, has to be improved which could therefore also lead to a modification of the final CMB map.

Still, a comparison of the ILC and (Hinshaw et al. 2007) low-ℓ multipoles does not reveal any major disagreement. If the microwave spectrum of the unknown dust cloud had significant variations, then it would have been removed, at least partially, by the ILC method and left intact by the Hinshaw et al. (2007) method, leading to substantial divergence between their results. The only way the cloud can stay hidden for both is if it has a nearly flat spectrum close to that of the CMB.

This leads us to the conclusion that if the anomalous multipoles are indeed caused by an unaccounted dust cloud, or if there is any cloud that adds an undesirable foreground, the cloud must have a relatively flat temperature spectrum between 3 and 14 mm. We return to a quantitative assessment of how flat the temperature spectrum needs to be, and what it implies for the cloud's particle composition and sizes, in Section 4.

3. THE THERMAL EMISSION BY HOMOGENEOUS SPHERICAL GRAINS

3.1. Excerpts from the Theory of Thermal Emission

Dust particles absorb, scatter, and emit electromagnetic radiation. Absorption and scattering lead to extinction of light from sources behind the particle, with the absorbed light heating up the particle. Also, scattering and emission add new light to the observer's line of sight, with the radiative energy being transferred from other directions and wavelengths, respectively.

The absorption efficiency $Q_{\rm abs}$, scattering efficiency $Q_{\rm sca}$ and extinction efficiency $Q_{\rm ext} = Q_{\rm abs} + Q_{\rm sca}$ are the ratios of the corresponding effective cross-sectional area to the geometric cross-sectional area of the particle. Knowing the radius a of a spherical particle, one can easily calculate the energy absorbed, scattered and removed from the radiation flux at a given wavelength.

The thermal emission of light by a particle is described in a more elaborate way using the thermal equilibrium equation:

$$\int_0^\infty \pi a^2 Q_{\rm abs}(a,\lambda)\mathcal{F}(\lambda)d\lambda = 4\int_0^\infty \pi a^2 Q_{\rm abs}(a,\lambda)B_\lambda(T_{\rm D})d\lambda, \quad (6)$$

where λ is the wavelength, $\mathcal{F}$ is the incident radiance flux, $B_\lambda(T_{\rm D})$ is the blackbody radiance at the dust particle's temperature $T_{\rm D}$. As the left-hand side provides the total energy absorbed from a monodirectional incident flux, the right-hand side gives the total energy emitted, omni-directionally. In the solar system, where the solar radiation is dominant, the incident radiance flux $\mathcal{F}$ can be safely replaced by the solar spectrum, which is close to a blackbody radiating at 5700 K, reduced at the distance R from the Sun by the factor $(R_\odot/R)^2$, where $R_\odot$ is the solar radius.

By denoting the absorption efficiency averaged over the solar spectrum with $\bar{Q}_\odot$, and the same quantity averaged over a blackbody spectrum at temperature $T_{\rm D}$ with $\bar{Q}(T_{\rm D})$, then using the Stefan–Boltzmann law and the solar constant, one can rewrite Equation (6) in a more concise form (cf. Reach 1988):

$$T_{\rm D} = 279{\rm K}[\bar{Q}_\odot/\bar{Q}(T_{\rm D})]^{1/4}R^{-1/2}, \quad (7)$$

where R is measured in AU. A perfect blackbody with $Q_{\rm abs} = 1$ throughout the spectrum has therefore a temperature of 279 K at 1 AU from the Sun, inversely proportional to the square root of the distance. This inverse-square-root trend is often closely followed by the real dust particles.

The Mie light scattering theory allows one to calculate the efficiencies $Q_{\rm abs}$, $Q_{\rm sca}$, and $Q_{\rm ext}$ as functions of particle radius a and wavelength λ once the refractive index is provided for the particle material (Bohren & Huffman 1983). The index of refraction is a complex number $m = n + {\bf i}k$, where the real part n is the inverse phase speed in the material with respect to the speed of light in vacuum, and the imaginary part k is the attenuation factor. The refractive index depends on wavelength. Under the assumption of homogeneity, it determines the propagation of electromagnetic waves inside the particle, while the assumption of spherical shape provides simplifications for determining the transformation of the waves at and near its boundary. The theory was formulated in the early 1900s in terms of the infinite series of spherical harmonic functions, its practical use was only made possible later on in the century by the development of computers. Standard Mie codes have been available to calculate the optical properties of particles based on the refractive indices.

A database of optical constants (Henning et al. 1999) provides plentiful bibliographic references and tables of the refractive indices necessary to predict the light-scattering properties of dust particles composed of various materials, in a wide range of wavelengths. Even though the microwave range is covered very sparsely, one can find a number of directions to the relevant laboratory studies and remote observations.

3.2. Particle Composition and Optical Constants

In our selection of materials, we followed partly the rationale of Reach (1988) for materials constituting solar system dust, largely supported by asteroid taxonomy. Carbonaceous particles are abundant in interstellar space and have been directly observed with the mass spectrometers onboard *Giotto* and *Vega-2* during the rendezvous with comet 1P/Halley in 1986 (Jessberger et al. 1988). Carbonaceous material covers the surfaces of C-type asteroids which is the dominant type in the asteroid belt, with 75% of known asteroids falling in this category. Silicate material largely constitutes the lunar and terrestrial rocks and was also revealed in the mass spectra of the 1P/Halley dust. It is abundant in circumstellar debris disks, allowing for remote studies of optical properties of silicate particles (Ossenkopf et al. 1992). 17% of known asteroids are of *S*-type, i.e., silicaceous according to their surface spectra. Even though the cosmic abundance of Fe is low, iron is the major component of some meteorites, magnetite (Fe_3O_4) is present in many of them. L-type asteroids, which constitute 7% of known asteroids show metallic surfaces. In more distant parts of the solar system not reviewed by Reach (1988), ice grains are an important population. Ice has been reported to cover the trans-Neptunian objects (see Brown et al. 1999; Jewitt & Luu 2004). The icy moons and rings of Jupiter and Saturn further support the case for including ice in our review. Therefore, we will focus ourselves on the optical properties of carbonaceous, silicate, iron and icy particles.

Ossenkopf et al. (1992) inferred the light scattering properties of the silicate grains from the opacities of circumstellar dust disks at the wavelengths of up to 10 mm. Between 1 and 10 mm, the real part of the refractive index stays near $n \approx 3$, while the imaginary part drops from $k \approx 0.025$ at the lower boundary to $k \approx 0.0025$ at the upper boundary of the range, inversely proportional to wavelength (Figures 4(a) and (b)). This is reported both for warm oxygen-deficient circumstellar silicates and cool oxygen-rich interstellar silicates considered in the paper.

The optical constants for silicate particles (Laor & Draine 1993; Figures 4(a) and (b)) differ only slightly from the values given by Ossenkopf et al. (1992), with a similar inverse phase speed $n = 3.4$ and an attenuation factor decreasing with wavelength at the same rate yet from a higher $k \approx 0.05$ at 1 mm. Note, however, that the Laor & Draine (1993) constants are not provided for $\lambda > 1$ mm and had to be extrapolated, assuming that the steep downward trend is continued in the microwaves.

The optical constants for olivine provided by Pollack et al. (1994), however, disagree with those of Ossenkopf et al. (1992) and a simple extrapolation of Laor & Draine (1993) beyond a wavelength of 1 mm. Ossenkopf et al. (1992) do not quote any observations beyond 1 mm. It is reasonable to assume that these authors extrapolated the trend seen in the far-infrared wavelength into the microwaves. In contrast, the constants for olivine by Pollack et al. (1994) are based on laboratory measurements by Campbell & Ulrichs (1969) at 8.57 mm and 66.7 mm who show that silicates do not gain transparency in the microwaves as fast as the extrapolations suggest. Boudet et al. (2005) may have found an explanation for the disagreement. They studied the temperature dependence of the absorption by amorphous silicate grains between 10 and 300 K and found that with increasing temperatures the absorption efficiency grows considerably (by an order of magnitude) already in submillimeter wavelengths. Therefore, the theoretical considerations behind the extrapolation by Ossenkopf et al. (1992) may still hold true for cold dust, whereas the Campbell & Ulrichs (1969) measurements in the warmth of a ground-based laboratory turn out to be more relevant to the near-Earth dust environment. Since our

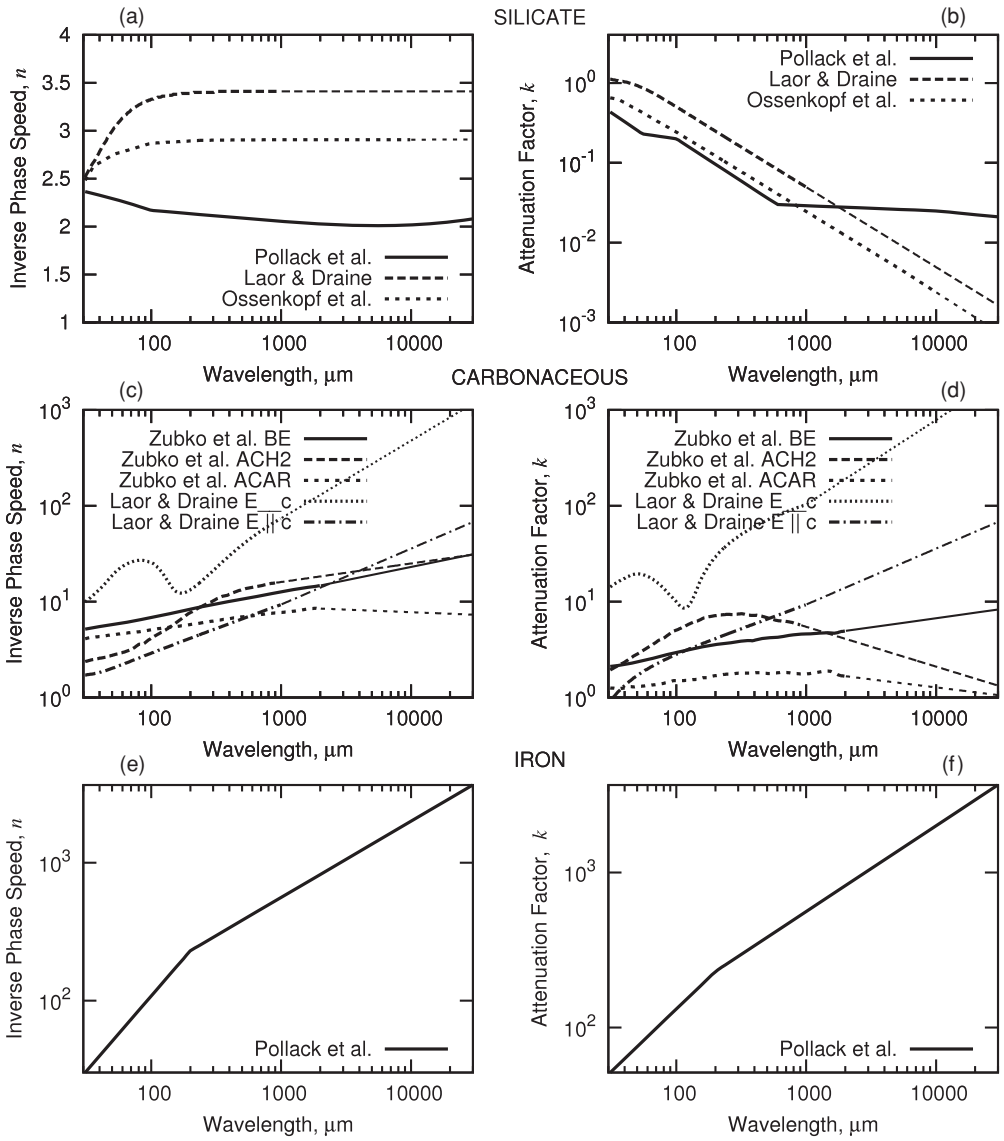

Figure 4. Optical constants for several chemical compositions of spherical homogeneous particles found in Pollack et al. (1994), Ossenkopf et al. (1992), Laor & Draine (1993), and Zubko et al. (1996). Top to bottom: silicate, carbonaceous, and iron particles. Thick curves are the data provided by the above authors, thin curves are our extrapolations. The solid curve in each plot emphasizes the variant that is chosen for further calculations of the absorption efficiencies and thermal emission.

main application of the Mie theory will be for a higher temperature, the Pollack et al. (1994) model is adopted as most reliable beyond 1 mm.

In contrast to silicates, the amorphous carbonaceous grains studied in the laboratory by Zubko et al. (1996) show much higher real parts of the refractive index n of up to ten and more, as well as imaginary parts k of several at the wavelengths near 1 mm (Figures 4(c) and (d)). The imaginary part of the refractive index does not fall but grows with increasing wavelength for the "BE" sample, i.e., amorphous carbon grains produced in burning benzene in air under normal conditions. Two other species studied by Zubko et al. (1996), those produced by arc discharge between amorphous carbon electrodes in different atmospheres ("ACAR" and "ACH2"), are characterized by the imaginary parts of the refractive indices reaching maxima between 100 and 1000 μm and then turning down. Nevertheless, as we have checked, they show qualitatively similar dependencies of the absorption efficiency on wavelength.

Additionally, the optical constants for graphite particles up to 1 mm wavelength are provided in the paper (Laor & Draine 1993; Figures 4(c) and (d)). The graphite particles behave similar to the above-listed species of amorphous carbon when the electric field vector is perpendicular to the plane of graphite cleaves (their "$E \parallel c$" explained in Draine & Lee 1984), while the particles with the cleaves being parallel to the field vector are significantly different ("$E \perp c$"). The absorption efficiency in the latter case is very low, however, making the thermal emission by a cloud of randomly oriented graphite particles well described by the first case.

We adopt for further calculations the optical constants of the "BE" sample (Zubko et al. 1996) as a reasonably good representation for the absorption efficiency of the above-listed carbonaceous species.

Zubko et al. (1996) have limited their study to wavelengths up to 2 mm, while our application of the Mie theory to the *WMAP* data requires the optical constants for up to ~10 mm. We have not found any constants for carbonaceous particles at $\lambda > 2$ mm in the literature. The optical constants of Zubko et al. (1996) are therefore extrapolated as shown in Figures 4(c) and (d) (thin lines).

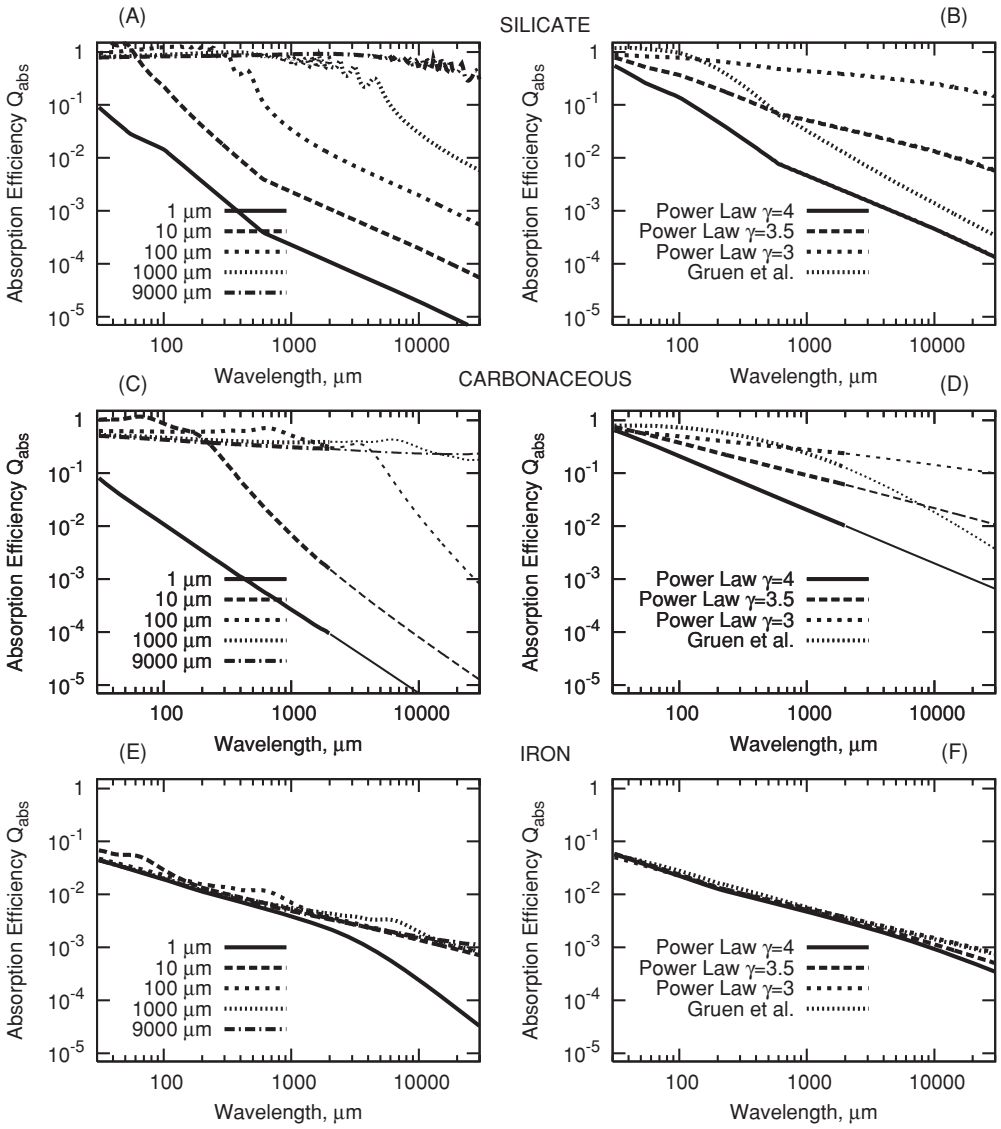

Figure 5. Absorption efficiencies of spherical homogeneous particles for the same chemical compositions as in Figure 4. From top to bottom: silicate, carbonaceous, and iron particles. Left column: absorption efficiencies for single particles of different sizes; right column: for size distributions $n(a)da = a^{-\gamma}da$ and the interplanetary meteoroid size distribution of Grün et al. (1985).

Iron particles (Figures 4(e) and (f)) have a rather plain dependence of the optical constants on wavelength (Pollack et al. 1994). As shown in that paper, qualitatively similar dependencies are also exhibited by iron combinations with some other elements, such as iron sulfide FeS, a circumstance that allows the results of the metallic iron model application to be expanded onto a correspondingly broader range of particle composition.

Water ice is reported to have $n \approx 1.8$ and k decaying from 10^{-2} at the wavelength of 1 mm to 10^{-3} at 10 mm, and at a temperature of $-1°$C (Warren 1984). For lower temperatures, k is lower: at $-60°$C, the values range from 3×10^{-3} at 1 mm to 3×10^{-4} at 10 mm. Solid ice can survive for a long time only far from the Sun, where the temperatures are low (see Equation (7)), e.g., $\sim$50 K $= -223°$C in the trans-Neptunian belt. The attenuation factors for cosmic ice can therefore be even lower than 10^{-4}. Then the grains absorb or emit virtually no microwave radiation, unless they are much bigger than the wavelength, i.e., centimeters in size. This is in agreement with Pollack et al. (1994), who show that the imaginary part decays from 3×10^{-3} to 3×10^{-4}, while the real part of the refractive index is in agreement with the value found by Warren (1984). It is noteworthy that CO_2 ice has a similar real part $n \approx 1.4$, whereas the imaginary part of the refractive index almost vanishes ($m < 10^{-6}$; Warren 1986). While the attenuation factor can be raised by impurities, it is generally fair to say that cosmic ice absorbs the microwave radiation negligibly with respect to carbons and even silicates. Therefore, we discuss neither water nor CO_2 ice in the remainder of the paper.

3.3. Calculation of Absorption Efficiencies

The absorption efficiencies for the particle compositions considered above, except for ice, are shown in Figure 5. The left panels show single-particle efficiencies, while in the right panels the efficiencies are averaged over different size distributions that can be expected in dust clouds.

Single-particle plots show a steep decrease of the absorption efficiencies of small grains with wavelength. Because the

attenuation factor sharply weakens with wavelength, the absorption efficiency is proportional to $Q_{\rm abs} \propto \lambda^{-2}$ for silicate particles of 1 μm radius between 100 and 600 μm wavelengths. If the optical constants by Ossenkopf et al. (1992) were adopted, this trend would continue to the microwaves. However, the flattening attenuation of Pollack et al. (1994) changes the trend somewhat above 600 μm. As the particle size grows, the absorption efficiency flattens too, with a roughly constant value for wavelengths shorter than the particle size.

The carbonaceous particles show an analogous qualitative behavior, however, due to much stronger attenuation, their absorption efficiencies are flat for λ less than $\sim 10a$. This is clearly seen for $\lambda < 2$ mm where the actual measurements have been used by Zubko et al. (1996) to determine the optical constants.

Interestingly, the absorption efficiencies of iron particles starting from ~ 10 μm in size are much less size dependent over the wavelength range under consideration. They also do not completely flatten up to the biggest size considered, i.e., ~ 10 mm, but instead all sizes above 10 μm share a weak dependence $Q_{\rm abs} \propto \lambda^{-1/2}$. Even though this decay is extremely weak in comparison with that of like-sized silicate and carbonaceous particles, it leads to the absorption efficiency vanishing to almost 10^{-3} at wavelength of several millimeters, which makes iron a very unlikely candidate for the elusive cloud material. For the sake of brevity it will not be considered during subsequent deliberations.

The size distributions assumed in our calculations include power laws $n(a)da = a^{-\gamma}da$ with several slopes γ, and the size distribution of interplanetary meteoroids (Grün et al. 1985) which was derived from the crater size distribution on lunar rock samples and remains the basis for the modern meteoroid environment models (Divine 1993; Staubach et al. 1997; Dikarev et al. 2005). The absorption efficiencies of single particles were averaged over the cross-sectional area using

$$\frac{\int Q_{\rm abs}(a,\lambda) n(a) a^2 da}{\int n(a) a^2 da}, \qquad (8)$$

where the integration limits were separated sufficiently to bracket all the dust that can emit at a given wavelength (tiny submicron-sized grains are inefficient already in infrared radiation, so e.g., for the Grün et al. 1985 distribution of interplanetary meteoroids in Figure 6(a) moderate growth of cross-sectional area in the grains with $s < 100$ nanometers is invisible; huge meter-sized boulders are too rare).

The slopes γ were picked around the Mathis–Rumpl–Nordsieck (MRN) distribution (Mathis et al. 1977) found for the interstellar dust and which are typical for many other dust clouds as well, i.e., $\gamma = 3.5$. This slope was also derived for the steady-state size distribution of a cloud of colliding and disrupting particles (Dohnanyi 1969). The slope can be modified by particle dynamics.

Figure 6 shows the size distributions used in our calculations as well as one of their momenta, the cross-sectional area distribution. Shallow slopes γ emphasize bigger particles in the cloud, and make the average absorption efficiency accordingly flatter. The interplanetary meteoroid size distribution by Grün et al. (1985) yields a steep absorption efficiency since the bulk of its cross-sectional is comprised by particles from 10 to 100 μm in size. The Grün et al. (1985) distribution has different slopes in various size ranges, where different dynamics determine distinct particle lifetimes: a slope close to 3.5 for $a < 1$ μm, near 2 between 1 and 100 μm, and about 5 above 100 μm.

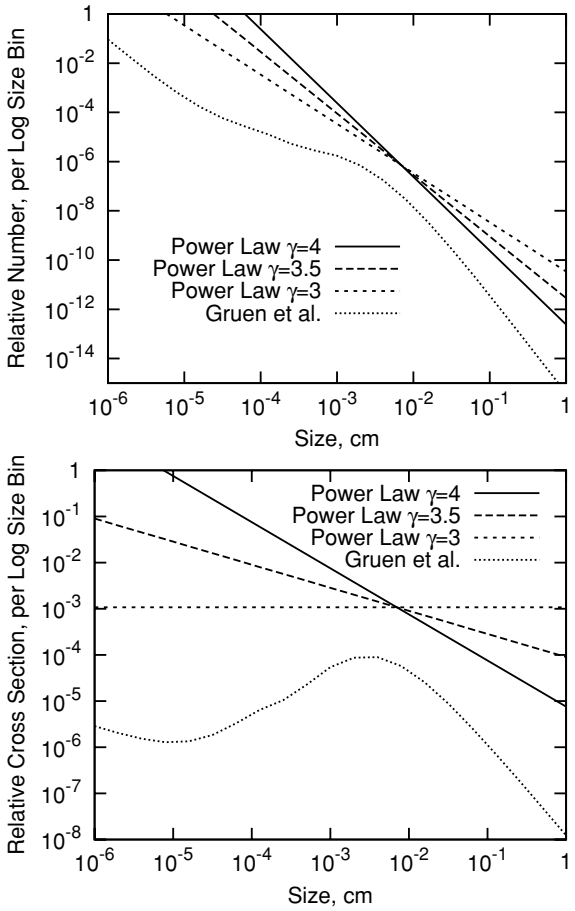

Figure 6. Size distributions $n(a)da = a^{-\gamma}da$ and the interplanetary meteoroid size distribution of Grün et al. (1985) used in producing the average absorption efficiencies in Figure 5 (top). The corresponding cross-sectional area distributions (bottom).

3.4. Nonsphericity and Inhomogeneity

The assumptions of sphericity and homogeneity made above for the sake of simplicity can of course be debated. Aggregates can indeed emit differently at long wavelengths, especially if they include conducting materials (carbon, iron). Interestingly, by taking the porosity into account one can come to flat absorption efficiencies for even smaller particles. Carbonaceous ballistic particle-cluster aggregates (PCAs) usually give flatter efficiencies than Mie spheres. The more realistic the method, the more pronounced is the effect: e.g., modified spectral function (MSF) predicts flatter efficiencies than discrete multipole method (DMM), and DMM flatter than effective-medium theories (EMTs; see e.g., Stognienko et al. 1995, for more details and references). Therefore, we have good reasons to trust that our Mie calculations provide results rather conservative with regard to flatness, which is important for our conclusions.

4. THE TEMPERATURE SPECTRA OF DUST CLOUDS

The column absorption area of a dust cloud is simply the product of its column cross-sectional area and the absorption efficiency of constituting particles. Assuming the column cross-sectional area equal to 10^{-7}, i.e., close to that of the zodiacal cloud near Earth, and taking $Q_{\rm abs}$ from Section 3, we calculated the corresponding temperature spectra (see Figure 7). The dust particle temperature was set to 300 K (cf. Equation (7)).

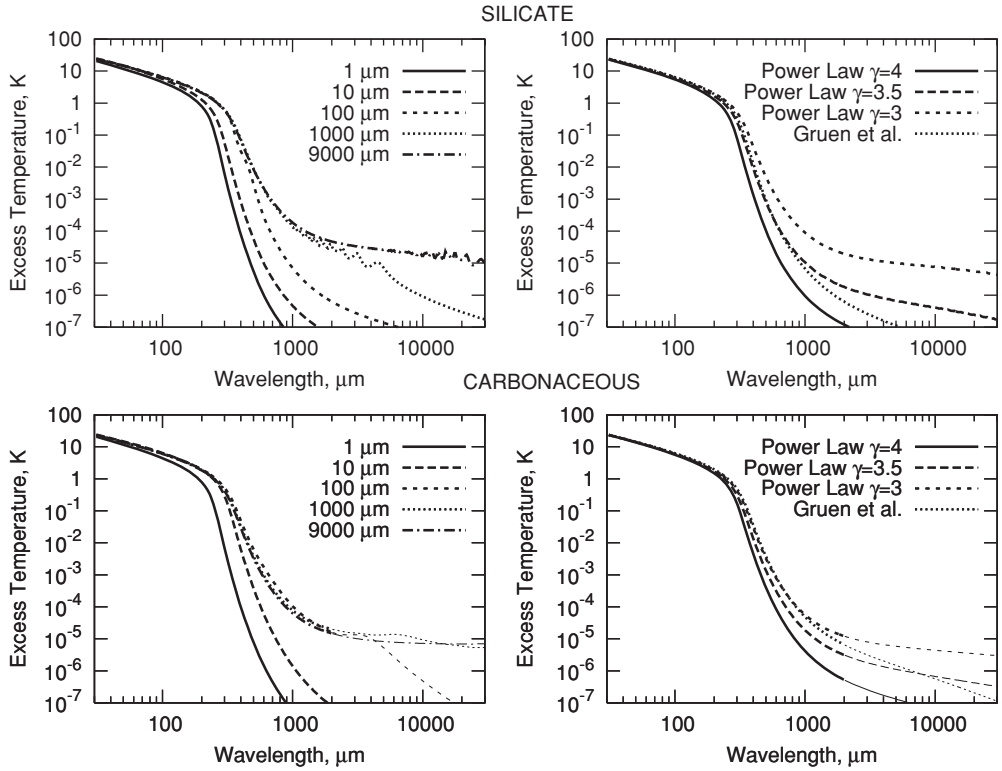

Figure 7. Temperature spectra of dust clouds composed of silicate (top) and carbonaceous (bottom) particles. Monosize clouds are displayed in the left column, size distributions as in Figure 5 are in the right column. A dust temperature of 300 K and column cross-sectional area of 10^{-7} were assumed, similar to those of the zodiacal cloud as seen from the Earth.

The peak of the blackbody emission at that temperature is near 10 μm, while the CMB maximum is near 1 mm. This leads to very high excess temperatures due to dust over the CMB at the short wavelengths. The temperature spectra of small, micrometer-sized particles drop sharply in the far-infrared and microwaves, however. In contrast, bigger particles show a pronounced flattening of temperature spectra if their size is similar to or bigger than the wavelength. The thermal emission by dust and the CMB is on the Rayleigh–Jeans side of their Planck functions above 1 mm wavelength, where they are approaching proportionality to temperature, and the temperature spectrum of dust is determined mainly by the absorption efficiency, which is flat for macroscopic particles. Silicate particles above several millimeters in radius exhibit flat temperature spectra, while the emission from carbonaceous grains larger than several hundreds of micrometers in size are already unaffected and thus not excluded by the ILC procedure.

It is important to note that the temperature of the dust cloud needs not necessarily be low to produce a flat temperature spectrum over the *WMAP* wavelengths. Cooling the dust particles, e.g., by moving them away to the trans-Neptunian belt (to 50 K) or even further to the Oort cloud, will by itself not make the temperature spectrum flat in the microwaves. Even warm (300 K) particles can give a rather flat spectrum if they are big. Simultaneously, due to their broadly flat emissivity, they do not reveal themselves at shorter wavelengths, in contrast to small micrometer-sized dust. Therefore, the big particles may easily be outshone by more abundant small particles in the infrared, yet dominate the microwave emission.

A proposal by Frisch (2005) that the thermal emission of interstellar dust trapped in the heliosphere is an explanation of the CMB anomalies can be rejected since the grains are too small, submillimeter in size. No matter how far they are from the Sun, due to a steep decrease of their absorption efficiencies with wavelength they would be rejected by the ILC map construction procedure, and visible in the infrared wavelengths.

Power-law size distributions of dust are characterized by flat temperature spectra only if their slope γ is weak, so that the big particles constitute the bulk of the cross-sectional area, according to our findings about monosize clouds. The Grün et al. (1985) size distribution of interplanetary meteoroids gives a temperature spectrum that is quite steep for the ILC if the meteoroids are silicate, shallower if the particles are carbonaceous.

Figure 8 zooms into the *WMAP* wavelength range. More particle sizes are plotted in the monosize cloud case to facilitate more accurate assessment of the temperature spectra. Note that the Grün et al. (1985) model's size distribution, when normalized to the zodiacal cloud visual optical depth (10^{-7}), is brighter than 1 μK up to 6 mm wavelength under the hypothesis that all meteoroids are carbonaceous (bottom right plot). At the shortest wavelength of *WMAP* (3 mm) it can be as bright as several μK. If indeed there are 5 times more big meteoroids in the interplanetary space outside the Earth's orbit (Section 2.1 and Figure 2) than in the flux at 1 AU, one can get up to $\sim$10 μK thermal emission in the microwaves. Of course, the uncertainties of the chemical composition and size distribution impact the accuracy of such estimates. Similarly, the trans-Neptunian belt estimated to have a geometrical optical depth of 2×10^{-7} in particles bigger than 1 cm, would provide $\sim$15 μK emission if it were fully carbonaceous ($Q_{\rm abs} \sim 0.5$ in Figure 5, cf. Section 2.1). This is not the case, as there are many ice particles in the belt which are not visible in the microwaves, however, the number is intriguingly high.

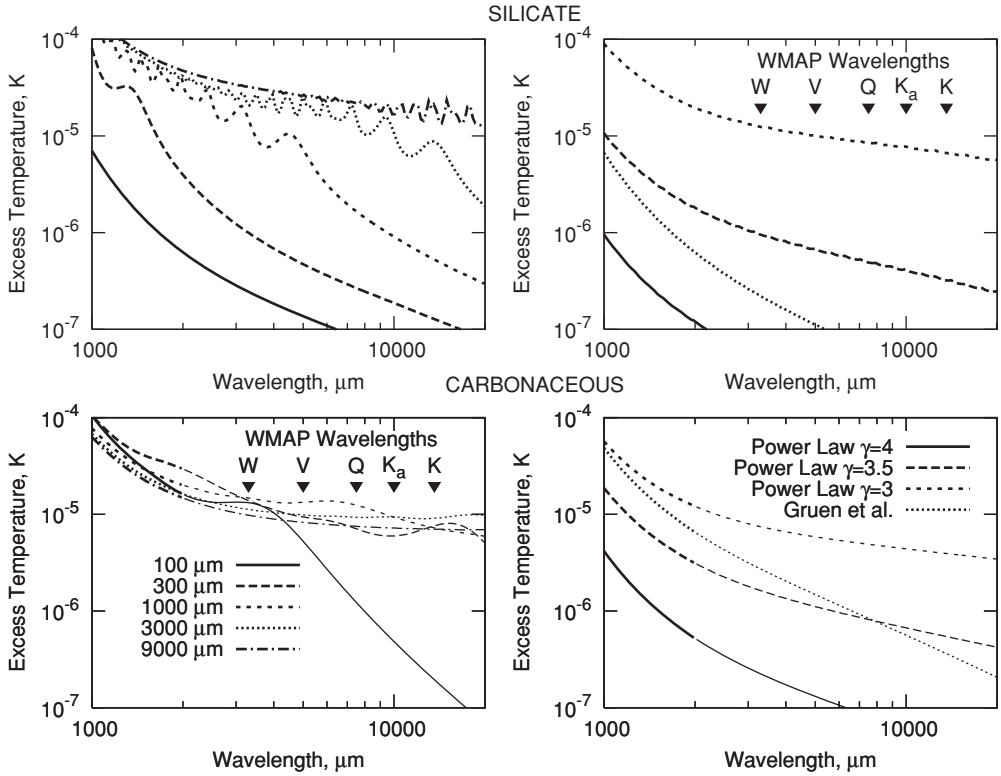

Figure 8. Zoom of Figure 7 into the *WMAP* wavelength range.

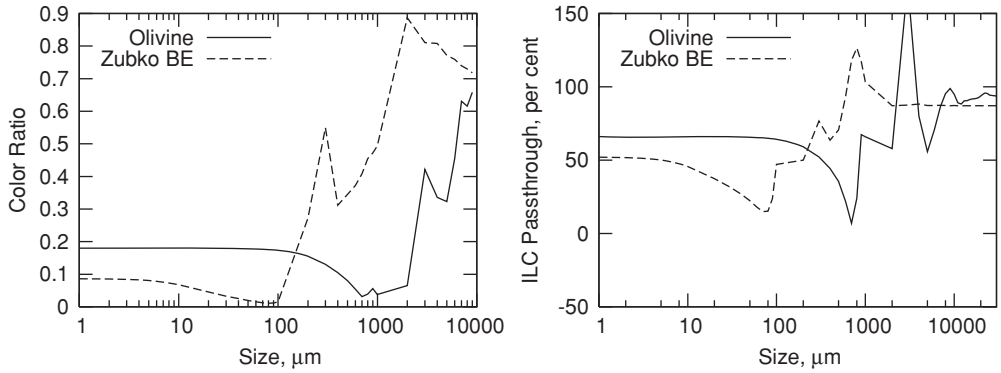

Figure 9. "Color ratio" (left) of olivine and carbonaceous particles as a function of their size. The color is defined as $T_{13.6}/T_{3.3}$, i.e., the ratio of temperatures of the cloud in 13.6 and 3.3 mm wavebands of the *WMAP* radiometers. ILC passthrough ratio (right), per cent, for monosize clouds of olivine and carbonaceous particles in region 1 (higher galactic latitudes). The ratio is a fraction of the cloud's emission that passes through the ILC bias correction procedure (Bennett et al. 2003b), to the total emission. The ratio can be above 100% as well as negative due to the peculiarities of the cloud spectrum.

The "color ratio" of monosize clouds is plotted in Figure 9 (left) as a function of size. It is the ratio of the excess temperatures of the clouds in the 13.6 to that in the 3.3 mm waveband, $\Delta T_{13.6}/\Delta T_{3.3}$. The color ratio of the carbonaceous particles of Zubko et al. (1996) rises to close to unity for a particle size between 1 and 2 mm, i.e., where reliable optical constants are still available. The color ratio for olivine remains low up to particle size of several mm. Obviously, in order to pass the ILC filter, one needs bigger silicate particles than carbonaceous ones. Interestingly, the color ratio of all power laws and interplanetary meteoroids of Grün et al. (1985) is too low, typically below 0.5.

We have also calculated how much emission from dust can pass through the ILC filters, assuming that the cloud is sufficiently "transparent" to leave the filter weights unaffected (i.e., determined by other foregrounds with higher brightness and/or steeper spectra). If the cloud were not "transparent," the weights would be affected and a fraction of the cloud emission would be removed, leading to a difference between the ILC and Hinshaw et al. (2007) foreground-cleaned maps, which is too low (Section 2.2). Clouds with higher passthrough ratios are therefore more plausible, even though not proven, candidates for sources of large unaccounted contaminations in the *WMAP* data. Note that clouds with low passthrough ratios would affect the ILC weights in a way that the ratios are further lowered.

Figure 9 (right) displays the passthrough ratio for the ILC weights derived for region 1 encompassing the higher galactic latitudes and most of the ecliptic plane. This is the largest region on the sky where one could be most eager to search for an unknown dust cloud since the galactic emission is minimal inside it. It is interesting to note that the emission from the clouds composed of olivine particles is reduced by about 30%

only if the particles are microscopic. Eriksen et al. (2004) had already emphasized that the ILC procedure is not very efficient in removing the emission from dust, although they found it more efficient than in our test: approximately half of the *W*-band (3.3 mm) simulated emission from dust was in their "cleaned" maps. They used the λ^{-2} emissivity which is steeper than that of olivine. In our test, carbonaceous material allows us to reduce the emission of clouds of microscopic particles by half.

The ILC passthrough test confirms the results of the color ratio test: olivine particles of about 10 mm in size and carbonaceous particles of roughly 1 mm in size reach a nearly 100% "transparency" for the bias removal procedure. However, one should bear in mind that monosize clouds are very rare in nature. A broad size distribution should allow clouds composed of smaller particles to become "transparent" too, as the sharp peaks and drops of the ILC passthrough at big sizes would cancel out after an averaging. The Grün et al. (1985) size distribution of interplanetary meteoroids has ILC passthroughs of 64% and 58% for carbonaceous and olivine particles, respectively. If, however, the big meteoroids are under-represented in the meteoroid flux at 1 AU, the percentages may be higher. Ignoring all meteoroids less than 100 μm in size, one can come to passthroughs of 95% (carbonaceous) and 55% (olivine). These numbers are directly attributable to the cloud of meteoroids from short-period comets discussed in Section 2.1. Note that for real non-spherical inhomogeneous particles, the percentages will likely be even closer to 100% (Section 3.4).

5. CONCLUSION

We have investigated the microwave thermal emission by dust in the solar system. We applied the Mie theory of light scattering by spherical homogeneous particles in order to characterize the thermal emission spectra of silicate, carbonaceous, iron and icy particles. Our study is partly motivated by the *WMAP* observations of the CMB fluctuations that revealed large-scale structures aligned with the solar-system geometry which are difficult to explain by the standard inflationary cosmology. One possibility of producing such fluctuations is by a dust cloud inside or in the vicinity of the solar system. Another motivation for this study is to assess the feasibility of detection of dust in and near the solar system in the microwaves.

We used the *WMAP* multi-wavelength observations and infrared surveys to constrain the physical properties of particles constituting the hypothetical cloud and to estimate the microwave emission by solar-system dust. We have found that only macroscopic, mm-sized silicate or carbonaceous grains could produce thermal emission with a spectrum compatible with that of the CMB fluctuations. Smaller dust grains, as well as iron particles, emit with a spectrum that can easily be distinguished from the CMB. The small particles would also be so bright in the infrared light that they would have been seen by the relevant telescopes, whereas the big particles have a flat emissivity throughout the spectrum, so that the abundant small grains outshine them at infrared wavelengths.

In order to attain the flat emissivity at the *WMAP* wavelengths, silicate particles must be several mm in size at least, whereas carbonaceous particles can be an order of magnitude smaller. This makes the carbonaceous particles the most likely candidate, as small grains are typically more likely in dust clouds than big ones. Meteoroids from short-period comets (Hughes & McBride 1990) are a plausible candidate for such cloud. The dust needs not necessarily be cold nor remote. When the cloud is composed of particles with a broad size distribution, even smaller dust grains can contribute to an overall flat spectrum without revealing themselves. For example, all particles of the Grün et al. (1985) meteoroid flux model with sizes above 100 μm have an integral spectrum sufficiently flat to pass the ILC procedure used to clean the *WMAP* observations from biases, if they are composed of carbonaceous material. The trans-Neptunian belt is another plausible candidate. According to our preliminary estimates, each candidate cloud can emit roughly $\sim$10 μK in the microwaves.

We found studies (see Stognienko et al. 1995, for references) showing that the Mie theory provides in general more pessimistic estimates of compatibility between the dust and CMB spectra than advanced light scattering theories taking nonsphericity and inhomogeneity into account. It means that the real particles can be even smaller than those quoted above in this conclusion.

There is a lack of measurements of the optical constants of carbonaceous particles above a wavelength of 2 mm. Given that this material provides the best chances so far to explain the *WMAP* anomaly, laboratory measurements of carbonaceous particles would be very helpful for further studies of the problem.

In subsequent papers of this series, using the thermal emission model introduced here, we will test the absolute photometry and projected geometry of various known and hypothetical dust clouds in and near the solar system, against the maps of CMB fluctuations made by *WMAP*.

Useful discussions with Dr. Harald Mutschke are greatly appreciated. Prof. Eberhard Grün's reading and commenting the manuscript were very helpful. We also thank an anonymous referee for very careful reading of the manuscript and a number of valuable suggestions that have improved the text and composition of the paper. This work has been (partially) supported by the WCU grant (No. R31-10016) funded by the Korean Ministry of Education, Science and Technology, and by the Deutsche Forschungsgemeinschaft (grant reference SCHW 1344/3 − 1).

REFERENCES

Babich, D., Blake, C. H., & Steinhardt, C. L. 2007, ApJ, 669, 1406
Bennett, C. L., et al. 2003a, ApJ, 583, 1
Bennett, C. L., et al. 2003b, ApJS, 148, 1
Bohren, C. F., & Huffman, D. R. 1983, Absorption and Scattering of Light by Small Particles (New York: Wiley)
Boudet, N., Mutschke, H., Nayral, C., Jäger, C., Bernard, J.-P., Henning, T., & Meny, C. 2005, ApJ, 633, 272
Brown, R. H., Cruikshank, D. P., & Pendleton, Y. 1999, ApJ, 519, L101
Campbell, M. J., & Ulrichs, J. 1969, J. Geophys. Res., 74, 5867
Copi, C. J., Huterer, D., Schwarz, D. J., & Starkman, G. D. 2006, MNRAS, 367, 79
Copi, C. J., Huterer, D., & Starkman, G. D. 2004, Phys. Rev. D, 70, 043515
Cornish, N. J., Spergel, D. N., Starkman, G. D., & Komatsu, E. 2004, Phys. Rev. Lett., 92, 201302
de Oliveira-Costa, A., Tegmark, M., Zaldarriaga, M., & Hamilton, A. 2004, Phys. Rev. D, 69, 063516
Dikarev, V., Grün, E., Baggaley, J., Galligan, D., Landgraf, M., & Jehn, R. 2005, Adv. Space Res., 35, 1282
Divine, N. 1993, J. Geophys. Res., 98, 17029
Dohnanyi, J. S. 1969, J. Geophys. Res., 74, 2431
Draine, B. T., & Lee, H. M. 1984, ApJ, 285, 89
Eriksen, H. K., Banday, A. J., Górski, K. M., & Lilje, P. B. 2004, ApJ, 612, 633
Finkbeiner, D. P., Davis, M., & Schlegel, D. J. 1999, ApJ, 524, 867
Frisch, P. C. 2005, ApJ, 632, L143
Fuentes, C. I., & Holman, M. J. 2008, AJ, 136, 83
Gordon, C., Hu, W., Huterer, D., & Crawford, T. 2005, Phys. Rev. D, 72, 103002
Gor'kavyi, N. N., Ozernoy, L. M., Mather, J. C., & Taidakova, T. 1997, ApJ, 488, 268

Grün, E., Zook, H. A., Fechtig, H., & Giese, R. H. 1985, Icarus, 62, 244
Hannestad, S., & Mersini-Houghton, L. 2005, Phys. Rev. D, 71, 123504
Henning, T., Il'In, V. B., Krivova, N. A., Michel, B., & Voshchinnikov, N. V. 1999, A&AS, 136, 405
Hinshaw, G., et al. 2007, ApJS, 170, 288
Hinshaw, G., et al. 2009, ApJS, 180, 225
Hughes, D. W., & McBride, N. 1990, MNRAS, 243, 312
Hunt, P., & Sarkar, S. 2004, Phys. Rev. D, 70, 103518
Ishimoto, H. 2000, A&A, 362, 1158
Jaffe, T. R., Banday, A. J., Eriksen, H. K., Górski, K. M., & Hansen, F. K. 2005, ApJ, 629, L1
Jessberger, E. K., Christoforidis, A., & Kissel, J. 1988, Nature, 332, 691
Jewitt, D. C., & Luu, J. 2004, Nature, 432, 731
Krivov, A. V., Müller, S., Löhne, T., & Mutschke, H. 2008, ApJ, 687, 608
Land, K., & Magueijo, J. 2005, Phys. Rev. Lett., 95, 071301
Laor, A., & Draine, B. T. 1993, ApJ, 402, 441
Leinert, C., et al. 1998, A&AS, 127, 1
Leinert, C., Roser, S., & Buitrago, J. 1983, A&A, 118, 345
Linde, A. 2004, J. Cosmol. Astro-Part. Phys., JCAP10(2004)004
Low, F. J., et al. 1984, ApJ, 278, L19
Maris, M., & Burigana, C. 2007, Mem. Soc. Astron. Ital. Suppl., 11, 83
Mathis, J. S., Rumpl, W., & Nordsieck, K. H. 1977, ApJ, 217, 425
Moffat, J. W. 2005, J. Cosmol. Astro-Part. Phys., JCAP10(2005)012
Mota, B., Gomero, G. I., Rebouças, M. J., & Tavakol, R. 2004, Clas. Quantum Grav., 21, 3361
Naselsky, P. D., Chiang, L.-Y., Novikov, I. D., & Verkhodanov, O. V. 2005, Int. J. Mod. Phys. D, 14, 1273
Ossenkopf, V., Henning, T., & Mathis, J. S. 1992, A&AS, 261, 567
Piao, Y.-S. 2005, Phys. Rev. D, 72, 103513
Pollack, J. B., Hollenbach, D., Beckwith, S., Simonelli, D. P., Roush, T., & Fong, W. 1994, ApJ, 421, 615
Reach, W. T. 1988, ApJ, 335, 468
Schlegel, D. J., Finkbeiner, D. P., & Davis, M. 1998, ApJ, 500, 525
Schwarz, D. J., Starkman, G. D., Huterer, D., & Copi, C. J. 2004, Phys. Rev. Lett., 93, 221301
Slosar, A., & Seljak, U. 2004, Phys. Rev. D, 70, 083002
Spergel, D. N., et al. 2007, ApJS, 170, 377
Starkman, G. D., & Schwarz, D. J. 2005, Sci. Am., 291, 36
Staubach, P., Grün, E., & Jehn, R. 1997, Adv. Space Res., 19, 301
Stognienko, R., Henning, T., & Ossenkopf, V. 1995, A&A, 296, 797
Sykes, M. V., & Walker, R. G. 1992, Icarus, 95, 180
Tegmark, M., de Oliveira-Costa, A., & Hamilton, A. J. 2003, Phys. Rev. D, 68, 123523
Warren, S. G. 1984, Appl. Opt., 23, 1206
Warren, S. G. 1986, Appl. Opt., 25, 2650
Wyatt, S. P., & Whipple, F. L. 1950, ApJ, 111, 134
Zubko, V. G., Krelowski, J., & Wegner, W. 1996, MNRAS, 283, 577